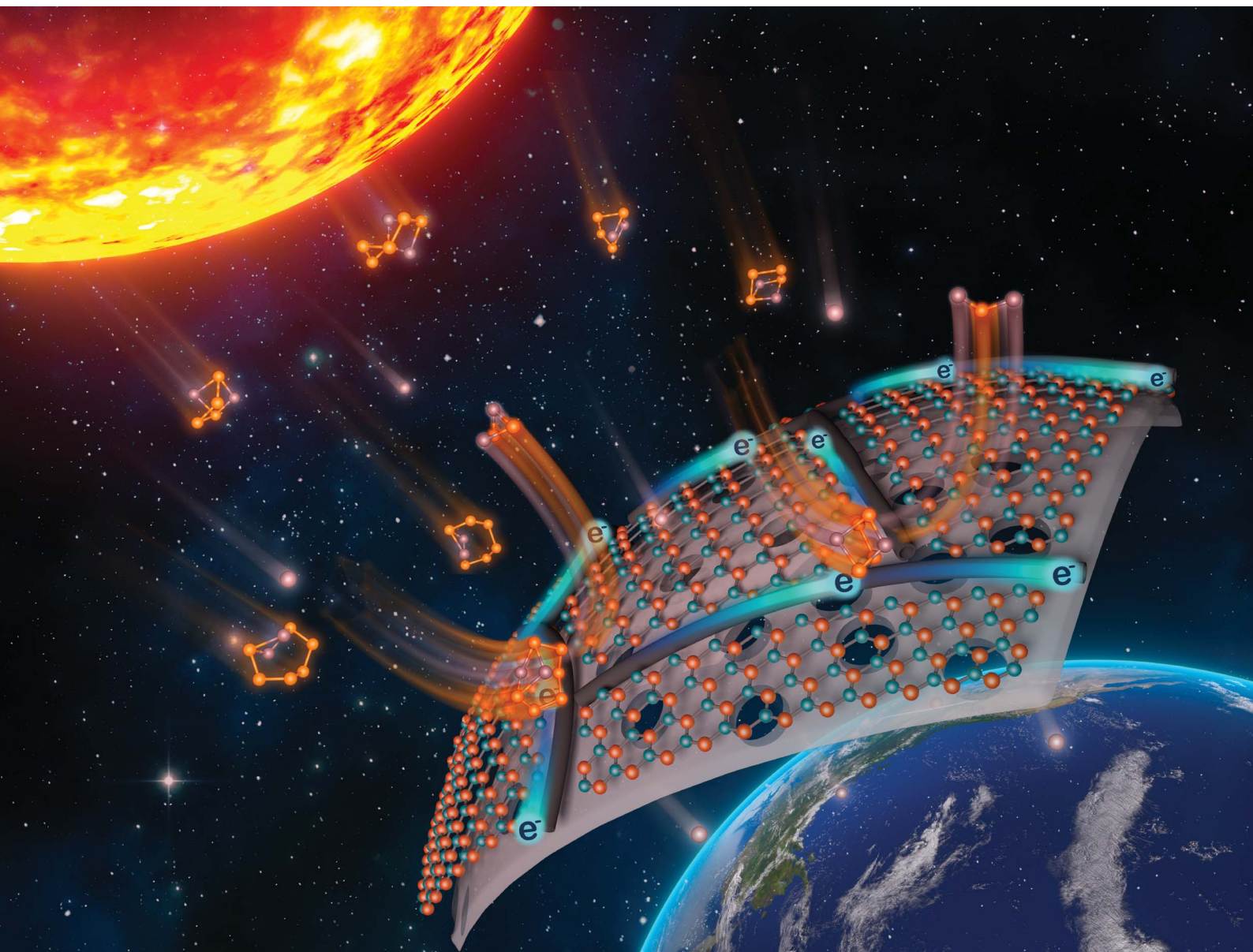


Journal of Materials Chemistry A

Materials for energy and sustainability

rsc.li/materials-a



ISSN 2050-7488

PAPER

Zhenhua Sun, Feng Li *et al.*

An ultrathin and highly efficient interlayer for lithium-sulfur batteries with high sulfur loading and lean electrolyte

Cite this: *J. Mater. Chem. A*, 2022, 10, 7653

An ultrathin and highly efficient interlayer for lithium–sulfur batteries with high sulfur loading and lean electrolyte†

Xialu Fan,^{ab} Yingqi Liu,^c Junyang Tan,^c Shan Yang,^{ad} Xiaoyin Zhang,^{ab} Bitu Liu,^{bc} Huiming Cheng,^{ae} Zhenhua Sun^{ab} and Feng Li^{abf}

Lithium–sulfur (Li–S) batteries are considered to have great potential due to their high theoretical specific energy and natural abundance of sulfur. However, the practical specific energy and cycle life of Li–S pouch cells are significantly hindered by thin sulfur cathodes, flooded electrolytes and excess Li metal anodes. Here, an ultrathin and highly efficient boron nitride/single-wall carbon nanotube (BN/SWCNT) interlayer (UHEI) achieves excellent Li–S pouch cell performance with high sulfur loading and a lean electrolyte. Compared with the reported interlayer materials, the UHEI can not only hinder the diffusion of polysulfides, but also promote further redox reactions and allow Li⁺ to pass through easily. Meanwhile, this UHEI can significantly improve lean electrolyte performance (E/S ratio of 8 $\mu\text{L mg}^{-1}$) and both high and low plateau capacities of Li–S batteries with a high sulfur loading (10 mg cm^{-2}). Moreover, a normalized “ratio of the areal loading interlayer to sulfur (I/S)” was proposed and two “interlayer efficiency index (IEI)” were obtained by using I/S to quantify the efficiency of interlayers at a certain current density and guide the design of high-efficiency interlayers. The IEI of our UHEI@PP is dozens of times higher than previously reported results. Li–S cells with UHEI@PP delivered a remarkable discharge capacity of 6.6 mA h cm^{-2} after 100 cycles at 0.2C for pouch cells (4.1 mg cm^{-2} per side, E/S ratio of 10 $\mu\text{L mg}^{-1}$). The work provides new insights into separator modification for the practical application of lithium–sulfur batteries in the future.

Received 7th December 2021
Accepted 28th January 2022

DOI: 10.1039/d1ta10444f

rsc.li/materials-a

Introduction

Lithium–sulfur (Li–S) batteries with a high theoretical specific energy of 2600 W h kg^{-1} and a high reversible capacity of 1675 mA h g^{-1} are considered to have great potential as next-generation batteries.¹ Unfortunately, the energy density of practical Li–S cells is far from the theoretical values resulting from the following factors, such as the electrical insulation nature of sulfur and $\text{Li}_2\text{S}/\text{Li}_2\text{S}_2$,² the large volume change of sulfur (almost 80%),³ the migration of soluble intermediate

product polysulfides (Li_2S_x , $4 \leq x \leq 8$)⁴ (shuttle effect) and the safety issues of the Li anode.^{5,6} Various approaches have been reported to address the above-mentioned issues.⁷ For instance, carbon-based materials,^{8–10} conductive polymers^{11–13} and metal oxides/sulfides/nitrides^{14–16} were used as sulfur hosts to enhance charge transfer, reduce the volume strain¹⁷ and suppress the shuttle effect.¹⁸ However, the synthetic processes of these cathodes are complex and costly.¹⁹ Meanwhile, most studies were evaluated under ideal conditions with a low sulfur loading cathode ($<2 \text{ mg cm}^{-2}$), flooded electrolytes (electrolyte/sulfur ratio, E/S ratio, is typically more than 20 $\mu\text{L mg S}^{-1}$) and a thick lithium metal anode.²⁰ Cells show a low specific capacity and short cycle life with increasing sulfur loading and decreasing electrolyte.^{5,6,57} Therefore, practical capacity and stability with high sulfur loading and a low E/S ratio are crucial for Li–S batteries.

In contrast, interlayers, which can suppress the shuttle effect and improve cycling stability, are considered as a promising pathway to industrial production.²¹ Porous carbon,²² carbon nanotubes (CNTs),^{23,24,58} reduced graphene oxide (rGO),²⁵ metal oxides/sulfides and carbides/nitrides (Al_2O_3 ,²⁶ TiO_2 ,¹⁴ V_2O_5 ,²⁷ MoS_2 ,²⁸ NbC ,²⁹ TiN ³⁰ etc.^{53–55}) were used as interlayers to hinder polysulfides, which can improve the performance of Li–S batteries. However, the excessive mass and thickness of an

^aShenyang National Laboratory for Materials Science, Institute of Metal Research, Chinese Academy of Sciences, Shenyang, 110016, China. E-mail: fli@imr.ac.cn; zhsun@imr.ac.cn

^bSchool of Materials Science and Engineering, University of Science and Technology of China, Hefei, 230026, China

^cShenzhen Geim Graphene Center, Tsinghua-Berkeley Shenzhen Institute, Tsinghua Shenzhen International Graduate School, Tsinghua University, Shenzhen 518055, China

^dSchool of Chemical Engineering, Sichuan University, Chengdu 610065, China

^eInstitute of Technology for Carbon Neutrality, Shenzhen Institute of Advanced Technology, Chinese Academy of Sciences, Shenzhen 518055, China

^fDalian National Laboratory for Clean Energy, Dalian 116023, China

† Electronic supplementary information (ESI) available. See DOI: 10.1039/d1ta10444f

interlayer can increase the use of electrolyte and decrease the practical energy density of Li-S cells. Moreover, standards or methods to evaluate the efficiency of interlayers or other non-active components are absent. Generally, an ultrathin, ultra-light and highly efficient interlayer is very essential for practical Li-S batteries.

Two-dimensional (2D) materials, such as graphene and hexagonal boron nitride (h-BN), have been extensively investigated in recent years.^{31,32} In particular, h-BN nanosheets with a unique hexatomic ring molecular structure, thermal stability and outstanding mechanical strength have been considered as a promising candidate for electrochemical energy storage.³¹ Meanwhile, h-BN nanosheets are not only composed of light atoms but can also offer adequate active sites for polysulfide adsorption.³³ Most importantly, electro-positive B atoms can combine with the S_n^{2-} of lithium polysulfides and electronegative N atoms can combine with Li^+ according to Lewis acid-base theory.³⁴ Therefore, with dual Lewis basic and acidic sites, h-BN nanosheets can not only hinder polysulfides as a physical barrier, but also be a more effective adsorbent than graphene.³⁵ However, their electronic insulation nature impedes their application as an interlayer. Carbon nanotubes (CNTs) are the most efficient electronic conductive substrate for sulfur species.⁹ Surrounding h-BN nanosheets with CNTs can significantly increase electronic conductivity and realize the reutilization of polysulfides. Moreover, the mixture of h-BN nanosheets and CNTs is a high Li^+ conductive material and can enable Li^+ transfer easily across the interlayer, leading to promoted redox kinetics and increased rate capability.³⁶

Herein, a nitride-BN nanosheet/carbon nanotube (BN/SWCNT) layer was used as an ultrathin and highly efficient interlayer (UHEI) with dual Lewis basic/acidic sites, high Li^+ conductivity and catalytic ability for polysulfide conversion for high sulfur loading/lean electrolyte Li-S batteries. As illustrated in Fig. 1a, b and 2h, this UHEI shows a few advantages: First, the UHEI is very thin, light and highly efficient, which significantly increases the practical specific capacity of the whole system. Second, the UHEI can suppress polysulfide diffusion and accelerate the conversion to Li_2S/Li_2S_2 , which is conducive to lean electrolytes and high sulfur loading performances. Third, the UHEI enables Li^+ transfer

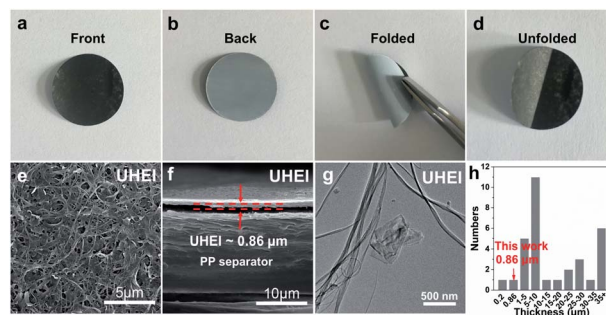


Fig. 2 Photos of UHEI@PP: (a) front side, (b) back side, (c) folded, and (d) unfolded. SEM images of (e) the surface of the UHEI and (f) cross-section of the UHEI. TEM images of (g) UHEI. (h) Thickness of various interlayers reported before.

easily across the interlayer, which significantly increases the redox kinetics of polysulfide conversion and improves the interlayer efficiency.

Experimental

Preparation of h-BN nanosheets

The fabrication process of h-BN nanosheets was reported previously.³⁷ Typically, the exfoliation of h-BN was carried out by grinding. First, 2 g bulk BN and 8 g SiC were mixed and placed inside a grinding cell. After grinding for 270 min, the as-ground mixture was dispersed into isopropanol (IPA), and the resulting solution was kept for 8 h. After that, green SiC and unexfoliated h-BN were precipitated at the bottom of the bottle and h-BN nanosheets dispersed stably in the supernatant. Therefore, the upper 3/4 supernatant was transferred by using a pipette and centrifuged to obtain the final h-BN dispersion.

Preparation of the UHEI

The UHEI was coated on a Celgard 2400 membrane (PP separator) by vacuum filtration. First, the as-obtained h-BN nanosheets were dispersed in IPA to obtain a mixed solution. Second, the SWCNT solution (0.4%, TUBALL) and the h-BN/IPA solution with a solute mass weight ratio of 1 : 3, were mixed under ultrasonication at 200 W for 20 min. Finally, the mixture was filtered through the PP separator and dried at 60 °C in a vacuum

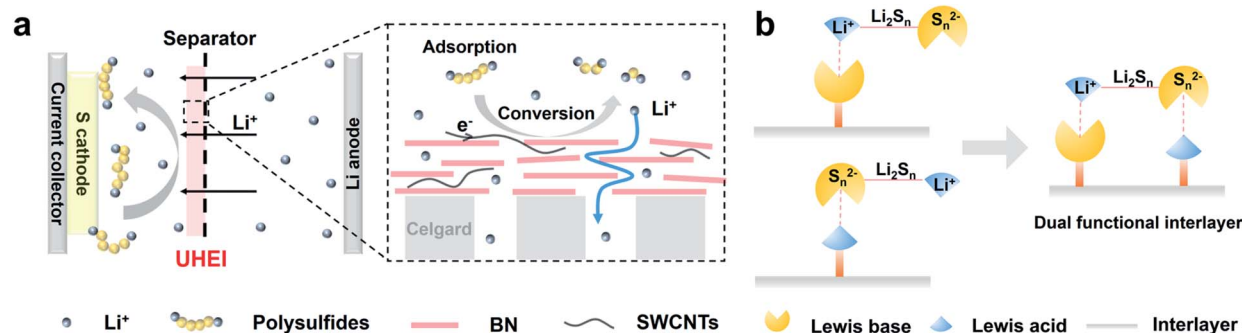


Fig. 1 Schematics showing (a) a Li-S battery with an UHEI and (b) the advantages of h-BN.

oven for 12 h, and denoted as UHEI@PP. The mass loading was kept at 0.17 mg cm^{-2} .

Preparation of the sulfur cathode

High sulfur loading cathodes (2.2 mg cm^{-2} , 5.3 mg cm^{-2} and 10.1 mg cm^{-2}) were obtained³⁸ without immersion in ammonium molybdate tetrahydrate ($(\text{NH}_4)_6\text{Mo}_7\text{O}_{24}\cdot 4\text{H}_2\text{O}$) aqueous solution. First, bacterial cellulose hydrogels purchased from Hainan Yida Food Industry Co., Ltd were washed with deionized water until neutral. Second, the hydrogels were frozen in liquid nitrogen and freeze-dried. Third, the dried aerogels were carbonized in an argon-filled tube furnace at $1000 \text{ }^\circ\text{C}$ for 2 h to produce a freestanding aerogel. Finally, the freestanding aerogel and sulfur powder (99.5%, Alfa Aesar) with different mass loadings were mixed in a Teflon container and heated to $155 \text{ }^\circ\text{C}$ for 12 h to obtain cathodes with high sulfur loading. A sulfur cathode for low electrolyte condition tests in coin cells was fabricated as follows. First, Super P (SP) and sulfur powder with a mass ratio of 3 : 7 were mixed in a Teflon container and heated to $155 \text{ }^\circ\text{C}$ for 12 h to obtain SP/S. Second, the SP/S, SP and polyvinylidene fluoride (PVDF) binder with a mass ratio of 7 : 2 : 1 was dispersed in *N*-methyl-2-pyrrolidone (NMP) to form a slurry. Finally, the slurry was coated onto a carbon-coated Al foil and dried in a vacuum oven at $60 \text{ }^\circ\text{C}$ for 12 h. The active material loading was kept at $1.5\text{--}2.0 \text{ mg cm}^{-2}$. The sulfur cathode for pouch cells was fabricated in the same manner under low electrolyte conditions, except the active material loading was kept at 4.1 mg cm^{-2} per side.

Permeation experiments of the UHEI@PP and PP separators

First, 1.6 g sulfur powder and 0.46 g lithium sulfide (99.5%, Alfa Aesar) were mixed and dissolved in 10 mL 1,2-dimethoxyethane (DME)/dioxolane (DOL) (volume ratio of 1 : 1). The mixture was stirred at $60 \text{ }^\circ\text{C}$ in a glove box to obtain the 1 M Li_2S_6 electrolyte. Second, the 1 M Li_2S_6 solution was diluted into 0.01 M and injected into the left chamber of an H-shaped device. The blank electrolyte was added into the right chamber at the same voltage. Finally, a UHEI@PP or PP separator was placed between the two chambers and digital photos were taken after 0.5 h, 24 h and 48 h.

Materials characterization

Scanning electron microscopy (SEM, FEI Nova NanoSEM 430, 10 kV) was used to characterize the morphologies and structures of the samples. Transmission electron microscopy (TEM) images were taken by using an FEI Titan ETEM G2 microscope at 80 kV and an FEI Tecnai F30 at 300 kV. The UV-Vis spectra were obtained by using a Varian 5000.

Preparation of Li-S coin cells

For coin cells, the sulfur cathode was cut into a square plate with a side length of 10 mm. The electrolyte was prepared by dissolving lithium bis-trifluoromethanesulphonylimide (LITFSI, 99%, Acros Organics, 1 M) and lithium nitrate (LiNO_3 , 99.9%, Alfa Asea, 0.1 M) in DME and DOL (1 : 1 by

volume). All cells were assembled in an Ar-filled glove box, with a sulfur cathode, Li foil, a UHEI@PP or PP separator, and the electrolyte mentioned above. The common electrolyte/sulfur (E/S) ratio in most coin cells was controlled to be $20 \mu\text{L mg}^{-1}$.

Preparation of Li-S pouch cells

Sulfur cathodes (4.1 mg cm^{-2} per side) and Li foil (0.1 mm thickness on Cu foil) of pouch cells were cut into 40 mm. A UHEI@PP or PP separator was placed between a sulfur cathode and a Li anode, and 3-layer Li-S pouch cells were obtained. The Al tab was ultrasonically welded on the as-prepared cathodes, and the Ni tab was ultrasonically welded on the Cu foil current collector. The electrolyte used in Li-S pouch cells is the same as that used in coin cells. Finally, the electrolyte ($\text{E/S} = 10 \mu\text{L mg}^{-1}$) was injected into the stack, and the package was sealed under vacuum.

Electrochemical measurements

The electrochemical performances were measured using coin and pouch cells. Galvanostatic charge/discharge tests were performed on a LAND galvanostatic charge/discharge instrument. The voltage range for charge/discharge was 1.7–2.8 V. 1C corresponding to 1675 mA g^{-1} . All experiments were performed at room temperature.

Results and discussion

The UHEI was uniformly coated on the PP separator by vacuum filtration, and no irreversible destruction could be observed after folding/unfolding tests (Fig. 2a–d), indicating a stable structure. The morphology of the pristine separator, BN and the UHEI were characterized by SEM. The surface of the pristine separator (Fig. S1a, ESI†) was full of slit pores with sizes of about hundreds of nanometers, while the UHEI completely covered the pores of the PP separator by overlapping hexagonal BN nanosheets (Fig. S1b†) and folded SWCNTs (Fig. 2e). The cross-sectional SEM image shows that the thickness of the UHEI is $0.86 \mu\text{m}$ (Fig. 2f), which is thinner than most interlayers reported^{19,25,31} (Fig. 2h). The TEM images show the h-BN nanosheets with a size of several micrometers (Fig. S1c†) and the SWCNTs surrounding the h-BN nanosheets (Fig. 2g). HRTEM images (Fig. S1d†) show that the lattice spacing of h-BN is 0.22 nm, corresponding to the (100) phase.

The permeation experiments of the UHEI@PP and PP separators were conducted by using an H-shaped device (Fig. 3a). The Li_2S_6 solution was injected into the left chamber, and the blank electrolyte was added into the right chamber. When UHEI@PP was placed between the two chambers, the color of the right side was nearly unchanged after 48 h. In contrast, after 0.5 h, the color of the side with the PP separator started to change to yellow and became much deeper after 24 h, conforming to the UV-Vis spectra (Fig. S3a†). The Li^+ transfer number and Li^+ conductivity are important for a separator with an interlayer. An ideal interlayer for Li-S batteries should be ion selective, which means that it should be polysulfide blocking, but Li^+ passing. Compared with the PP separator (0.66),

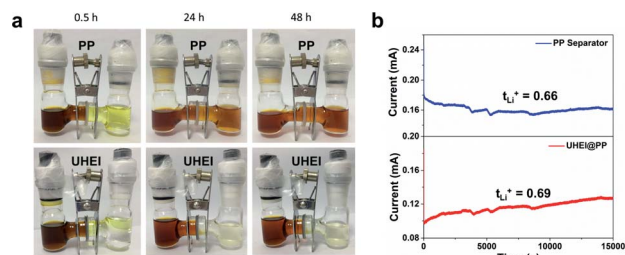


Fig. 3 (a) Polysulfide diffusion process of the PP separator and UHEI@PP. (b) Li^+ transference number of the PP separator and UHEI@PP.

UHEI@PP (0.69) shows almost the same Li^+ transfer number (Fig. 3b) and Li^+ conductivity (Fig. S3b and Table S1†).

To demonstrate the properties of UHEI@PP, Li-S coin cells were assembled with a high sulfur loading cathode, Li plate anode and UHEI@PP or PP separator. High sulfur loading cathodes were fabricated and charged/discharged at 0.1C rate.³⁸ With sulfur loading from 2.2 mg cm^{-2} to 10.1 mg cm^{-2} , Li-S batteries with UHEI@PP maintain two well-defined plateaus, while cells with a PP separator present nearly no plateau, especially with a sulfur loading of 10.1 mg cm^{-2} (Fig. 4a–c). The cycling stability and coulombic efficiency of Li-S batteries with an UHEI@PP or a PP separator at 0.1C with different sulfur loadings further demonstrate significant improvement in the capacity and stability of Li-S batteries with UHEI@PP (Fig. 4d–f). According to the redox reaction of the two plateaus mentioned above, the capacity ratio of each plateau represents the contribution of UHEI@PP during each S_8 redox reaction process. Bar graphs were used to visualize them (Fig. 5a and c). With a sulfur loading of 2.2 mg cm^{-2} , 5.3 mg cm^{-2} , or 10.1 mg cm^{-2} , the high plateau (2.35 V) UHEI@PP/PP ratio (the specific capacity of Li-S batteries with an UHEI@PP at 2.35 V divided by the specific capacity with a PP separator) is 1.32, 1.83, and 16.95, respectively, which depends on the redox of S_8 to long chain lithium polysulfides, mostly up to the electronic conductivity of the cathode and interlayer.³⁹ Obviously, UHEI@PP improved the electrochemical kinetics of the high plateau reaction

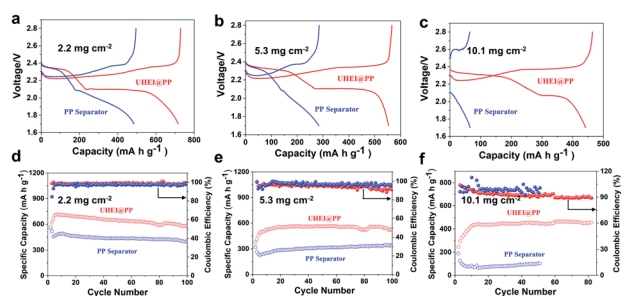


Fig. 4 Charge/discharge profiles of Li-S batteries with an UHEI@PP or a PP separator at 0.1C with sulfur loading of (a) 2.2 mg cm^{-2} , (b) 5.3 mg cm^{-2} , and (c) 10.1 mg cm^{-2} . The cycling stability and coulombic efficiency of Li-S batteries with an UHEI@PP or a PP separator at 0.1C with sulfur loading of (d) 2 mg cm^{-2} , (e) 5.3 mg cm^{-2} , and (f) 10.1 mg cm^{-2} .

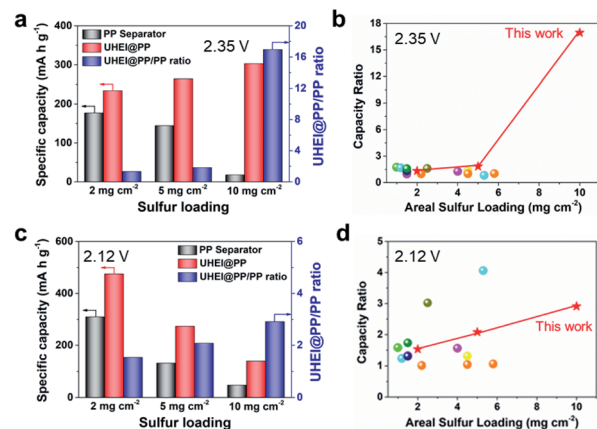


Fig. 5 (a) The high plateau specific capacities and the UHEI@PP/PP ratio of Li-S batteries with an UHEI@PP and PP separator with different sulfur loadings at 0.1C (the UHEI@PP/PP ratio is the specific capacity of Li-S batteries with an UHEI@PP divided by the specific capacity with a PP separator). (b) Comparison of high plateau capacity ratios with different sulfur loadings of our UHEI@PP with other interlayers in previous reports. (c) The low plateau specific capacities and the UHEI@PP/PP ratio of Li-S batteries with an UHEI@PP and PP separator with different sulfur loadings at 0.1C. (d) Comparison of low plateau capacity ratios with different sulfur loadings of our UHEI@PP with other interlayers in previous reports (★: this work, ●: P/C–C–N–Co (the single-atom cobalt-anchored nitrogen-doped carbon nanosheets and dual network of the carbon nanotube-cellulose nanofiber hybrid),⁴⁰ ●: CGF (mesoporous cellular graphitic framework),⁴¹ ●: NCM (NbC-coated membrane),²⁹ ●: ZnHMT (zinc-hexamethylenetetramine coordination complex),⁴² ●: μ FGF–MoS₂/C–TiN (microfiber glass filter-molybdenum disulfide/carbon-titanium nitride),⁴³ ●: ZnS/NCNS (zinc sulfide nanoparticles embedded in nitrogen-doped 3D-carbon nanosheets),⁴⁴ ●: TiB₂@G (metallically conductive TiB₂ coupled with two-dimensional graphene),⁴⁵ ●: PZI (polymeric zwitterion)⁴⁶).

process, especially with a high sulfur loading. The low plateau (2.12 V) UHEI@PP/PP ratio (the specific capacity of Li-S batteries with UHEI@PP at 2.12 V divided by that of Li-S batteries with a PP separator) is 1.53, 2.08, and 2.91, which represents the contribution of UHEI@PP during the redox of lithium polysulfides to Li_2S_2/Li_2S .³⁹ The increase in the low plateau (2.12 V) UHEI@PP/PP ratio further demonstrates that UHEI@PP not only adsorbs more polysulfides, but also promotes the polysulfide redox process, especially with a high sulfur loading. The comparison of each plateau capacity ratio of our UHEI@PP and other interlayer materials previously reported is illustrated in Fig. 5b, d and Table S2.† Cells with the UHEI@PP show excellent performances both from the two plateau capacity and the overall capacity aspects compared to those with other interlayer materials, especially at a high sulfur loading.

As we all know, the conversion of Li_2S_4 to Li_2S is challenging at high sulfur loading and the reasons can be summarized as follows: First, with the increase in areal sulfur loading, more polysulfides will accumulate and the concentration gradient force will increase, which make the shuttle effect more crucial. Second, the accumulated polysulfides will separate from the conductive frame and dissolve into the electrolyte, which further increases the electrolyte viscosity and impedes the

electrochemical reaction. Third, the polysulfides shuttled to the anode side will react with lithium metal and result in the passivation of the lithium anode. Therefore, a highly efficient interlayer with abundant polysulfide adsorption sites that can not only adsorb the accumulated polysulfides but also convert them to the final products is significant for high sulfur loading Li-S batteries.

To further illustrate the properties of UHEI@PP under low electrolyte conditions (E/S ratio of $8 \mu\text{L mg}^{-1}$), Li-S half cells with a UHEI@PP or PP separator were charged/discharged at 0.1C. Cells with UHEI@PP can maintain a reversible capacity of 1124 mA h g^{-1} (2^{nd} cycle) and have an ultralow capacity fading rate of 0.30% per cycle at 0.1C under lean electrolyte conditions (Fig. S6†). Meanwhile, a double side coated Li-S pouch cell with an average areal sulfur loading of 4.1 mg cm^{-2} per side was tested at 0.2C with an E/S ratio of $10 \mu\text{L mg}^{-1}$. A high reversible areal capacity of 6.6 mA h cm^{-2} was retained after 100 cycles, which is nearly twice as high as the areal capacity of the state-of-the-art $\text{LiNi}_x\text{Co}_y\text{Mn}_{1-x-y}\text{O}_2$ cathode (Fig. 6a). The fluctuating coulombic efficiency of the pouch cell with a UHEI can be attributed to the following reasons: First, the pouch cells with a UHEI were tested at a low E/S ($10 \mu\text{L mg}^{-1}$) ratio, which will lead to awful electrolyte infiltration and increased polysulfide viscosity in the sulfur cathode side. These two conditions contribute to the low utilization of polysulfides and a low coulombic efficiency. Second, the low N/P ratio exacerbates the effect of polysulfides on the lithium anode, which leads to a decrease in the coulombic efficiency. Third, unlike coin cells, the pouch cells with a UHEI were tested without any pressure. The literature reported before⁵² demonstrated that high pressure was proven to improve the sulfur cathode connectivity and avoid cracking over cycling with high sulfur loading, which is beneficial to sulfur utilization and coulombic efficiency. Finally, the reaction heterogeneity in Li-S pouch cells leads to a fluctuating coulombic efficiency.⁴⁷

Currently, most researchers focus on reducing the thickness of the interlayer materials and the proportion of the interlayer materials in all components to increase the energy density of the whole cells, but pay little attention to the efficiency of the interlayers. Typically, superior electrochemical performance has been reported to illustrate the efficiency of interlayers. However, considering objective factors among different studies (such as different compositions of cathodes), it is more convincing to compare the performance divergence with and without an interlayer. Moreover, an interlayer should be normalized based on unit active materials to ensure that the intrinsic effect of the interlayer is exhibited. Hence, a normalized “ratio of areal loading of the interlayer to sulfur (I/S)” was proposed, and the “interlayer efficiency index (IEI)” was obtained by using I/S to quantify the efficiency of the interlayers at a certain current density. A schematic of a Li-S pouch cell with a multilayer sulfur cathode (double side coating) and lithium anode is shown in Fig. S6a.† To simplify the analysis, a simple model with Cu foil, a lithium anode, a separator, an interlayer, a sulfur cathode, and Al foil is presented for calculation and discussion (Fig. S6b†). In this model, all components in the two Li-S pouch cells were supposed to be the same except the UHEI@PP or PP separator. As shown in Table S3,† the normalized I/S ratio was obtained by calculating the ratio of the areal loading of the interlayer and sulfur. I/S was used to normalize the performance divergence with and without an interlayer at a certain current density to obtain the IEI. One IEI (H_{mass}) calculated from the energy density of pouch cells was obtained as:

$$H_{\text{mass}} = \frac{E_{\text{with interlayer}}}{E_{\text{without interlayer}} \times I/S}$$

corresponding to the increased ratio of gravimetric energy density per mass (g) interlayer based on 1 g sulfur in pouch cells. In this equation, E is the energy density of a Li-S cell upon

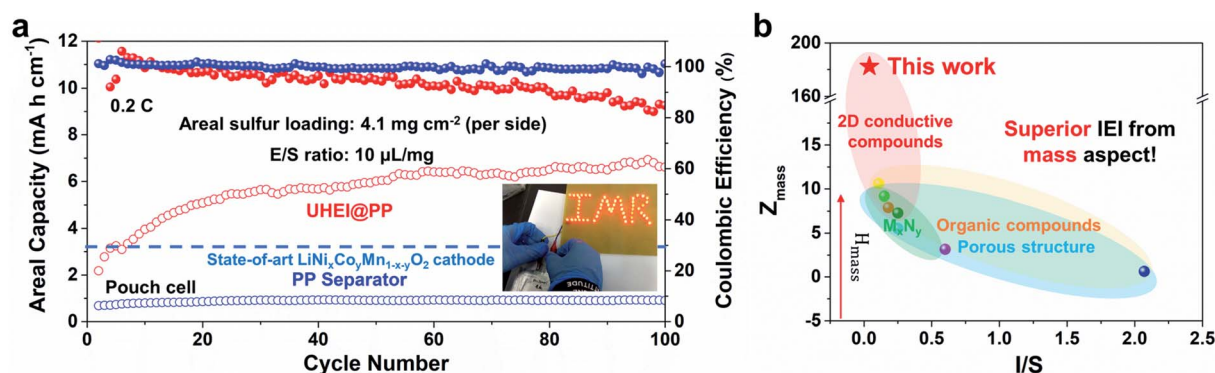


Fig. 6 (a) Cycling stability and coulombic efficiency of Li-S pouch cells with the UHEI@PP and PP separator at 0.2C with a high sulfur loading (4.1 mg cm^{-2} per side, double sides) and lean electrolyte (E/S ratio = $10 \mu\text{L mg}^{-1}$) for 100 cycles. (b) Comparison of the IEI and I/S of our UHEI@PP with previous reports from the specific capacity (Z_{mass}) aspect (★: this work, ●: CGF (mesoporous cellular graphene framework, Advanced Science, 2016),⁴¹ ●: NCM (NbC-coated membrane, Advanced Functional Materials, 2018),²⁹ ●: ZnHMT (zinc-hexamethylenetetramine coordination complex, Journal of Materials Chemistry A, 2020),⁴² ★: AS PC-Sn₄P₃ (acorn shell porous carbon/Sn₄P₃ nanodot, Nano Energy, 2020),³⁹ ●: HC-PDDA (poly(diallyl dimethyl ammonium chloride) on honey comb-like porous carbon, Energy Storage Materials, 2021),⁴⁹ ●: PPZ-HG-CCP (polyphosphazene covalently modified holey graphene/carbonized cellulose paper, Advanced Materials, 2021),⁵⁰ ●: PM (0.4 M)-CNT (porous Mxene membrane, Small, 2021),⁵¹ M_xN_y: (M: metal, N: nonmetal)).

discharge under specified conditions (W h kg^{-1}).⁴⁸ However, not all interlayers reported before were tested in pouch cells. Therefore, the IEI (Z_{mass}) was proposed to simplify H_{mass} . Z_{mass} was calculated from the practical specific capacity of coin cells as:

$$Z_{\text{mass}} = \frac{Y_{\text{with interlayer}}}{Y_{\text{without interlayer}} \times I/S}$$

corresponding to the increased ratio of practical specific capacity by per mass (g) interlayers based on 1 g sulfur in coin cells. In this equation, $Y_{\text{with interlayer}}$ is the practical specific capacity based on sulfur (mA h g^{-1}) with interlayer materials, and $Y_{\text{without interlayer}}$ is the practical specific capacity based on sulfur (mA h g^{-1}) with a PP separator. More details are available in the ESI.†

In this work, $Y_{\text{with interlayer}}$ is $794.1 \text{ mA h g}^{-1}$, $Y_{\text{without interlayer}}$ is $108.9 \text{ mA h g}^{-1}$, I/S is 0.041 , and Z_{mass} is 182.30 . The comparison of the IEI from the specific capacity aspect of our UHEI@PP and other interlayers previously reported are illustrated in Fig. 6b and Table S3.† Fig. 6b shows the relationship between the I/S and the IEI of different studies. The Z_{mass} of our UHEI@PP at 0.2C after 100 cycles is dozens of times higher than those of previous reports, which demonstrates its superior “interlayer efficiency”. Moreover, by proposing these factors, the following considerations can be achieved. First, with a similar electrochemical performance improvement, the smaller the I/S is, the better the efficiency of the interlayer is. Second, with a similar Z_{mass} , lowering the mass percentage of interlayers in all components gives a higher H_{mass} . Third, with a similar I/S , a lighter interlayer provides more adsorption sites which promotes better electrochemical performance improvement. Finally, 2D conductive compounds with polar adsorption sites and low density promote a higher IEI. Based on these indications, more efficient interlayers will be designed and used for high performance Li-S batteries. Similar deduction methods can be used to evaluate the efficiency of other non-active components in Li-S batteries. Therefore, this work may bridge the gap between lab-scale research and industrialization.

Conclusion

In summary, an ultrathin and ultra-light UHEI with dual-functional lithium polysulfide adsorption sites was prepared for high sulfur loading/lean electrolyte Li-S batteries. Meanwhile, a normalized coefficient, the ratio of areal loading of the interlayer to sulfur (I/S), was proposed and an interlayer efficiency index was obtained by using I/S to quantify the efficiency of interlayers at a certain current density. Compared with other reported interlayer materials, the UHEI can not only hinder polysulfide diffusion but also promote redox reactions and allow Li^+ to pass through easily. Our UHEI@PP can significantly improve the lean electrolyte performance (E/S ratio of $8 \mu\text{L mg}^{-1}$) and both the high and low plateau capacities of Li-S batteries with a high sulfur loading (10 mg cm^{-2}). Moreover, the IEI of our UHEI@PP is dozens of times higher than that of previous reports. Li-S batteries with UHEI@PP delivered a remarkable discharge capacity of 6.6 mA h cm^{-2} after 100

cycles at 0.2C for pouch cells (4.1 mg cm^{-2} per side, E/S ratio of $10 \mu\text{L mg}^{-1}$). The IEI offers a pathway for the design of high sulfur loading/lean electrolyte Li-S batteries, which could be extended to other electrochemical energy storage systems.

Conflicts of interest

There are no conflicts to declare.

Acknowledgements

This work was supported by the National Natural Science Foundation of China (No. 52020105010 and 51972313), the Strategic Priority Research Program of Chinese Academy of Science (No. XDA22010602), the Youth Innovation Promotion Association of the Chinese Academy of Sciences (No. Y201942), the Liaoning Revitalization Talents Program (No. XLYC1908015 and XLYC2007080) and the DNL Cooperation Fund, CAS (DNL202019).

Notes and references

- X. Liu, J. Q. Huang, Q. Zhang and L. Q. Mai, *Adv. Mater.*, 2017, **29**, 25.
- X. Tao, J. Wang, C. Liu, H. Wang, H. Yao, G. Zheng, Z. W. Seh, Q. Cai, W. Li, G. Zhou, C. Zu and Y. Cui, *Nat. Commun.*, 2016, **7**, 11203.
- P. G. Bruce, S. A. Freunberger, L. J. Hardwick and J. M. Tarascon, *Nat. Mater.*, 2012, **11**, 19–29.
- X. Ji, K. T. Lee and L. F. Nazar, *Nat. Mater.*, 2009, **8**, 500–506.
- Y. Sun, N. Liu and Y. Cui, *Nat. Energy*, 2016, **1**, 16071.
- W. Xue, Z. Shi, L. Suo, C. Wang, Z. Wang, H. Wang, K. P. So, A. Maurano, D. Yu, Y. Chen, L. Qie, Z. Zhu, G. Xu, J. Kong and J. Li, *Nat. Energy*, 2019, **4**, 374–382.
- M. Zhao, B. Q. Li, H. J. Peng, H. Yuan, J. Y. Wei and J. Q. Huang, *Angew. Chem., Int. Ed.*, 2020, **59**, 12636–12652.
- S. H. Chung, C. H. Chang and A. Manthiram, *ACS Nano*, 2016, **10**, 10462–10470.
- R. Fang, G. Li, S. Zhao, L. Yin, K. Du, P. Hou, S. Wang, H.-M. Cheng, C. Liu and F. Li, *Nano Energy*, 2017, **42**, 205–214.
- J. Liang, Z.-H. Sun, F. Li and H.-M. Cheng, *Energy Storage Mater.*, 2016, **2**, 76–106.
- G. Hu, Z. Sun, C. Shi, R. Fang, J. Chen, P. Hou, C. Liu, H. M. Cheng and F. Li, *Adv. Mater.*, 2017, **29**, 1603835.
- Z. B. Liang, C. Qu, W. H. Guo, R. Q. Zou and Q. Xu, *Adv. Mater.*, 2018, **30**, 39.
- C. Y. Chen, H. J. Peng, T. Z. Hou, P. Y. Zhai, B. Q. Li, C. Tang, W. Zhu, J. Q. Huang and Q. Zhang, *Adv. Mater.*, 2017, **29**, 1606802.
- Z. Wei Seh, W. Li, J. J. Cha, G. Zheng, Y. Yang, M. T. McDowell, P.-C. Hsu and Y. Cui, *Nat. Commun.*, 2013, **4**, 1331.
- J. Mei, T. Liao, L. Z. Kou and Z. Q. Sun, *Adv. Mater.*, 2017, **29**, 25.
- Z. Sun, J. Zhang, L. Yin, G. Hu, R. Fang, H. M. Cheng and F. Li, *Nat. Commun.*, 2017, **8**, 14627.

- 17 F. Hao, Z. X. Liu, P. B. Balbuena and P. P. Mukherjee, *ACS Appl. Mater. Interfaces*, 2019, **11**, 13326–13333.
- 18 R. Fang, K. Chen, L. Yin, Z. Sun, F. Li and H.-M. Cheng, *Adv. Mater.*, 2019, **31**, 1800863.
- 19 L. Tan, X. Li, Z. Wang, H. Guo and J. Wang, *ACS Appl. Mater. Interfaces*, 2018, **10**, 3707–3713.
- 20 J. Guo, H. Pei, Y. Dou, S. Zhao, G. Shao and J. Liu, *Adv. Funct. Mater.*, 2021, **31**, 2010499.
- 21 J. Y. Wu, X. W. Li, H. X. Zeng, Y. Xue, F. Y. Chen, Z. G. Xue, Y. S. Ye and X. L. Xie, *J. Mater. Chem. A*, 2019, **7**, 7897–7906.
- 22 Y.-S. Su and A. Manthiram, *Nat. Commun.*, 2012, **3**, 1166.
- 23 S.-H. Chung and A. Manthiram, *J. Phys. Chem. Lett.*, 2014, **5**, 1978–1983.
- 24 X. L. Fan, L. Q. Ping, F. L. Qi, Z. A. Ghazi, X. N. Tang, R. P. Fang, Z. H. Sun, H. M. Cheng, C. Liu and F. Li, *Carbon*, 2019, **154**, 90–97.
- 25 F. Wu, S. Y. Zhao, J. Li, Y. Lu, Y. F. Su, L. Chen, L. Y. Bao, J. Y. Yao and X. X. Liu, *ACS Appl. Mater. Interfaces*, 2019, **11**, 12544–12553.
- 26 Z. Zhang, Y. Lai, Z. Zhang, K. Zhang and J. Li, *Electrochim. Acta*, 2014, **129**, 55–61.
- 27 W. Li, J. Hicks-Garner, J. Wang, J. Liu, A. F. Gross, E. Sherman, J. Graetz, J. J. Vajo and P. Liu, *Chem. Mater.*, 2014, **26**, 3403–3410.
- 28 Z. A. Ghazi, X. He, A. M. Khattak, N. A. Khan, B. Liang, A. Iqbal, J. Wang, H. Sin, L. Li and Z. Tang, *Adv. Mater.*, 2017, **29**, 1606817.
- 29 W. L. Cai, G. R. Li, K. L. Zhang, G. N. Xiao, C. Wang, K. F. Ye, Z. W. Chen, Y. C. Zhu and Y. T. Qian, *Adv. Funct. Mater.*, 2018, **28**, 11.
- 30 T. H. Zhou, W. Lv, J. Li, G. M. Zhou, Y. Zhao, S. X. Fan, B. L. Liu, B. H. Li, F. Y. Kang and Q. H. Yang, *Energy Environ. Sci.*, 2017, **10**, 1694–1703.
- 31 D. R. Deng, C. D. Bai, F. Xue, J. Lei, P. Xu, M. S. Zheng and Q. F. Dong, *ACS Appl. Mater. Interfaces*, 2019, **11**, 11474–11480.
- 32 X. Cai, Y. Luo, B. Liu and H. M. Cheng, *Chem. Soc. Rev.*, 2018, **47**, 6224–6266.
- 33 Y. Fan, Z. Yang, W. Hua, D. Liu, T. Tao, M. M. Rahman, W. Lei, S. Huang and Y. Chen, *Adv. Energy Mater.*, 2017, **7**, 1602380.
- 34 S. Yuan, J. L. Bao, L. Wang, Y. Xia, D. G. Truhlar and Y. Wang, *Adv. Energy Mater.*, 2016, **6**, 1501733.
- 35 Y. Zheng, H. Li, H. Yuan, H. Fan, W. Li and J. Zhang, *Appl. Surf. Sci.*, 2018, **434**, 596–603.
- 36 Z. A. Ghazi, L. Zhu, H. Wang, A. Naeem, A. M. Khattak, B. Liang, N. A. Khan, Z. Wei, L. Li and Z. Tang, *Adv. Energy Mater.*, 2016, **6**, 1601250.
- 37 B. Liu, H.-M. Cheng, X. Zou, X. Cai, Y. Pan, J. Tan and C. Zhang, *Natl. Sci. Rev.*, 2020, **7**, 324–332.
- 38 H. Shi, Z. Sun, W. Lv, S. Wang, Y. Shi, Y. Zhang, S. Xiao, H. Yang, Q.-H. Yang and F. Li, *J. Mater. Chem. A*, 2019, **7**, 11298–11304.
- 39 Z. Ye, Y. Jiang, T. Feng, Z. Wang, L. Li, F. Wu and R. Chen, *Nano Energy*, 2020, **70**, 104532.
- 40 Y. Li, P. Zhou, H. Li, T. Gao, L. Zhou, Y. Zhang, N. Xiao, Z. Xia, L. Wang, Q. Zhang, L. Gu and S. Guo, *Small Methods*, 2020, **4**, 1900701.
- 41 H. J. Peng, D. W. Wang, J. Q. Huang, X. B. Cheng, Z. Yuan, F. Wei and Q. Zhang, *Adv. Sci.*, 2016, **3**, 1500268.
- 42 X. Dou, G. Li, W. Zhang, F. Lu, D. Luo, W. Liu, A. Yu and Z. Chen, *J. Mater. Chem. A*, 2020, **8**, 5062–5069.
- 43 M. Waqas, Y. Han, D. Chen, S. Ali, C. Zhen, C. Feng, B. Yuan, J. Han and W. He, *Energy Storage Mater.*, 2020, **27**, 333–341.
- 44 Z. Li, F. Zhang, L. Tang, Y. Tao, H. Chen, X. Pu, Q. Xu, H. Liu, Y. Wang and Y. Xia, *Chem. Eng. J.*, 2020, **390**, 124653.
- 45 L. Jin, J. Ni, C. Shen, F. Peng, Q. Wu, D. Ye, J. Zheng, G. Li, C. Zhang, Z. Li and J. P. Zheng, *J. Power Sources*, 2020, **448**, 227336.
- 46 G. Li, F. Lu, X. Dou, X. Wang, D. Luo, H. Sun, A. Yu and Z. Chen, *J. Am. Chem. Soc.*, 2020, **142**, 3583–3592.
- 47 L. Shi, S.-M. Bak, Z. Shadike, C. Wang, C. Niu, P. Northrup, H. Lee, A. Y. Baranovskiy, C. S. Anderson, J. Qin, S. Feng, X. Ren, D. Liu, X.-Q. Yang, F. Gao, D. Lu, J. Xiao and J. Liu, *Energy Environ. Sci.*, 2020, **13**, 3620–3632.
- 48 Y. T. Liu, S. Liu, G. R. Li and X. P. Gao, *Adv. Mater.*, 2021, **33**, 2003955.
- 49 H. Gao, S. Ning, J. Lin and X. Kang, *Energy Storage Mater.*, 2021, **40**, 312–319.
- 50 P. Chen, Z. Wu, T. Guo, Y. Zhou, M. Liu, X. Xia, J. Sun, L. Lu, X. Ouyang, X. Wang, Y. Fu and J. Zhu, *Adv. Mater.*, 2021, **33**, 2007549.
- 51 D. Xiong, S. Huang, D. Fang, D. Yan, G. Li, Y. Yan, S. Chen, Y. Liu, X. Li, Y. Von Lim, Y. Wang, B. Tian, Y. Shi and H. Y. Yang, *Small*, 2021, **17**, 2007442.
- 52 P. R. Chinnam, L. Xu, L. Cai, N. L. Cordes, S. Kim, C. M. Efav, D. J. Murray, E. J. Dufek, H. Xu and B. Li, *Adv. Energy Mater.*, 2021, 2103048.
- 53 Y. Qiu, X.-J. Yin, M.-X. Wang, M. Li, X. Sun, B. Jiang, H. Zhou, D.-Y. Tang, Y. Zhang, L.-S. Fan and N.-Q. Zhang, *Rare Met.*, 2021, **40**, 3147–3155.
- 54 J. Liu, Y. Cao, J. Zhou, M. Wang, H. Chen, T. Yang, Y. Sun, T. Qian and C. Yan, *ACS Appl. Mater. Interfaces*, 2020, **12**, 54537–54544.
- 55 Y. Li, X.-T. Guo, S.-T. Zhang and H. Pang, *Rare Met.*, 2021, **40**, 417–424.
- 56 M. A. Pope and I. A. Aksay, *Adv. Energy Mater.*, 2015, **5**, 1500124.
- 57 Z.-L. Xu, J.-K. Kim and K. Kang, *Nano Today*, 2018, **19**, 84–107.
- 58 J.-Q. Huang, Z.-L. Xu, S. Abouali, M. Akbari Garakani and J.-K. Kim, *Carbon*, 2016, **99**, 624–632.